PAPER Nr. : 18

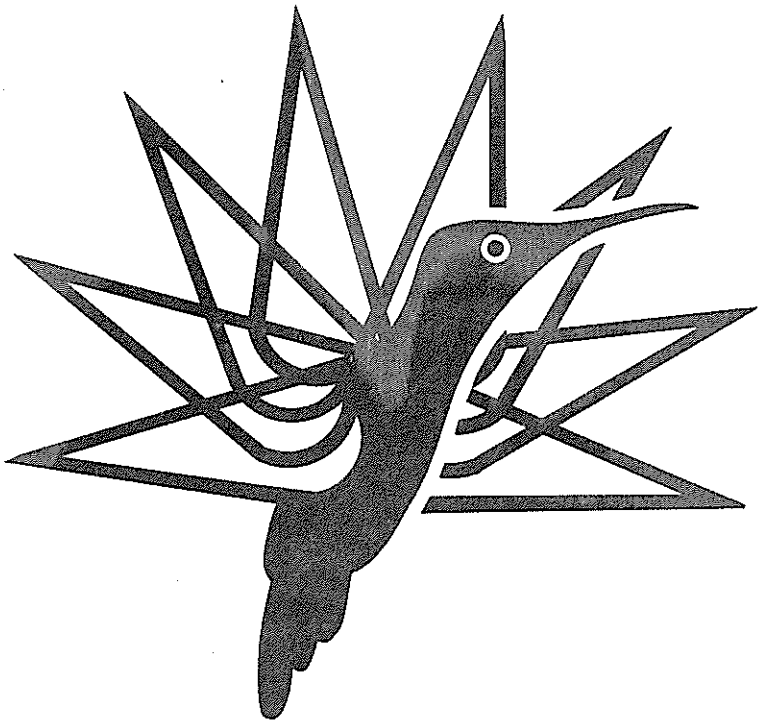

THE MEASUREMENT AND INTERPRETATION OF ROTOR BLADE PRESSURES AND LOADS ON A PUMA HELICOPTER IN FLIGHT

by

P. Brotherhood and C. Young
Structures Department
Royal Aircraft Establishment
Farnborough, Hampshire, England

FIFTH EUROPEAN ROTORCRAFT AND POWERED LIFT AIRCRAFT FORUM
SEPTEMBER 4 – 7TH 1979 - AMSTERDAM, THE NETHERLANDS

THE MEASUREMENT AND INTERPRETATION OF ROTOR BLADE PRESSURES AND LOADS ON A PUMA HELICOPTER IN FLIGHT

P. Brotherhood and C. Young
Structures Department
Royal Aircraft Establishment
Farnborough, Hampshire, England

ABSTRACT

A flight programme was initiated with the basic aim of providing data to validate in detail and extend the methods for predicting helicopter rotor performance and loads.

Three particular areas are addressed, the first being incidence distribution inferred from measurement of upper surface pressure close to the leading edge and corresponding data from two-dimensional oscillatory aerofoil tests. Particular emphasis was placed on a detailed radial definition of pressure from the middle of the blade outwards to the tip. Theoretical and experimental incidence distributions are compared and in particular the location of tip vortex paths.

The second area of interest is the distribution of stall boundaries based on a criteria of trailing edge pressure divergence and finally the comparison of measured and predicted blade oscillatory bending moments before and during retreating blade stall.

An animated ciné film of results has been prepared from the computer and associated Visual Display Unit.

1 INTRODUCTION

This paper describes work that is currently in progress at the Royal Aircraft Establishment aimed at validating and extending the methods used in the UK for the prediction of rotor loads and performance. An important part of this activity comprises flight experiments using a Puma helicopter as a test vehicle during which blade surface pressures and structural loads are measured. A large amount of test data has already been accumulated and the object of this paper is to illustrate the various ways in which it is being used. Most of the records have been taken in straight flight with the emphasis on rotor conditions approaching and during retreating blade stall, but more recently, a programme of manoeuvring flight including transients has been flown.

The flights so far have been made without a direct reading of aerodynamic sideslip for the pilot. The inertial slip-ball indicator was considered adequate in the high speed regime of flight which initially was of primary interest. The final phase of tests is continuing with a nose-boom mounted windvane fitted to the aircraft to resolve certain unexplained features in the results described later.

In this present paper only the results from rectilinear flight are discussed, that is those in which the initial conditions are better defined and more repeatable, and the theoretical modelling is least complicated.

Three particular areas are addressed, the first being the distribution of incidence inferred from the measurements of upper surface pressure close to the leading edge of the blade. Interpretation of the flight measurements is assisted by the results of two-dimensional oscillatory aerofoil tests from wind-tunnel experiments. Particular emphasis has been placed on a detailed radial

distribution of pressure and inferred incidence. Theoretical and experimental incidence distributions are compared to allow the important effects of local blade-tip vortex interactions to be defined. Improvements to the theoretical wake model can then be made particularly with regard to the spacial distribution of tip vortices in the horizontal plane.

The second area of interest is the distribution of stall boundaries within the rotor disc based on a criterion of trailing edge pressure divergence. Again, a close radial spacing of transducers was employed and experimental and theoretical results are compared.

The third area of interest is the comparison of the predicted oscillatory bending moments with those obtained from strain gauge measurements. The development of accurate prediction methods is essential for blade design and for estimating the vibratory input to the fuselage.

The planning of the test program and the complementary wind tunnel experiments were designed to identify the particular areas of disagreement and give pointers to some possible improvements in the prediction methods.

It is convenient to describe the main elements of the theoretical model and the comparison of the blade bending moments before the two topics mentioned previously, but before doing so, a brief account of the instrumentation and test procedure is given.

2 INSTRUMENTATION AND TEST PROCEDURE

Pressure transducers were installed in the upper surface of one of the four blades at 2% and 91% chord at 17 radial locations along the outer half of the blade (Fig 1). A smooth blade profile was maintained by recessing the leading edge transducers in shallow depressions in the blade spar. These and other modifications increased the rate of fatigue damage and shortened the blade life. Therefore the integrity of the blade had to be carefully and continuously monitored by means of strain gauge measurements at specified points on the blade. The trailing edge pressure transducers were recessed into the rear pockets of the blade. The flight conditions flown have included many points outside the normal aircraft flight envelope and more recently at reduced rotor speed giving much increased values of thrust coefficient. Consequently the 22 hours of flying so far completed have consumed the equivalent of some 450 hours of normal flight with unmodified blades.

The leading edge pressures were intended to give an indication of local blade incidence, with the trailing edge pressure divergence marking the onset of separation. Since the pressure at any point of the aerofoil in steady conditions is a function of Mach number and incidence, the incidence is uniquely defined by the pressure reading if the Mach number is known. This only applies during attached flow and a more complex relationship exists on a rotor blade where oscillatory conditions apply. Fig 2 shows the variation of leading and trailing edge pressure coefficients with incidence during attached flow for a Mach number relevant to the retreating blade. The leading edge pressure shows a simple hysteresis about the near linear quasi-steady test condition. Fig 3 shows a similar result but at a higher value of Mach number and provides data for the interpretation of flight results given in a later section. Fig 4 corresponds to a case at $M = 0.3$ with penetration into stall. Here the leading edge pressure has a nearly linear relationship with increasing incidence leading to an abrupt peak at about 16° accompanied by an almost simultaneous trailing edge pressure divergence; both parameters showing pronounced hysteresis particularly during the early stages of reducing incidence. The nonlinear behaviour makes a quantitative assessment of incidence difficult to achieve in certain circumstances, but it is still possible to obtain valuable qualitative information to define

regions of rapid increase and decrease of incidence. The onset of trailing edge pressure divergence also remains an indicator of stall during oscillatory conditions.

The structural loads in the blade for comparison with prediction were measured by strain gauges giving the flatwise bending moment at 35, 45, 55, 65, 75, 83, 90 and 95% radius, and strain gauges at 33% and 73% radius measured the edgewise and torsional moments. The blade root motion and the usual aircraft state and control parameters were also measured.

The rotor data was recorded on magnetic tape with a complete data frame every 1.5° in azimuth. Easy access to the data is provided through a specially developed computer program and interactive call-up procedure using a visual display. A wide range of analogue forms of data presentation is available with the ability to produce a permanent copy or a listing of the numerical data in tabular form. Interpretation of results is also helped by the use of a ciné camera photographing the visual display to produce animated film of selected sequences.

In the results presented, aerodynamic sideslip is assumed zero. As mentioned in the introduction the tests were flown with slip-ball zero. In order to balance the side force from the tail rotor, the direction of rotation of the main rotor dictates a tendency for left aerodynamic sideslip even when flown slip-ball centre, although the error may be minimised by initial canting of the instrument in the aircraft. Tests have recently been made with a trailing anemometer enabling an accurate correlation of slip-ball and associated lateral accelerometer readings with aerodynamic sideslip acquired from the lateral trail angle of the cable. The effect of aerodynamic sideslip on indicated airspeed was also obtained. However because of instrumentation difficulties, these tests were made without the experimental rotor blade fitted and not in conditions of retreating blade stall. The results indicate left sideslip of 4° and 2° when flown slip-ball zero at advance ratios of 0.17 and 0.32 respectively, conditions which are discussed in detail later. It is probable that these relatively small values of sideslip will increase during retreating blade stall at high thrust coefficient obtaining at lower than normal rotor speed, because of the additional tail rotor thrust required to balance the increased main rotor torque. Future tests with a nose-boom mounted windvane will help to quantify this effect.

3 THE PREDICTION OF ROTOR STRUCTURAL LOADS AND COMPARISON WITH MEASUREMENT

The method of calculating the performance of a rotor and the blade structural loads was developed mainly by Westland Helicopters Ltd. under contract. It uses a series of coupled modes, and the forced response equations are solved by a forward integration technique based on the Z-transform. The *in vacuo* modes are determined by an extension of the method of Hubolt and Brooks[2].

The rotor inflow can be calculated from the simple Glauert formula or by the more complicated vortex ring model. The downwash distribution in the vortex ring model is calculated by integrating the velocities induced by a series of root and tip vortex rings displaced horizontally and vertically from the tip path plane to represent the undistorted helical path of the wake. The strength of the root and tip vortices is equal but of opposite sign, and takes a constant value with a superimposed first harmonic variation approximating the varying load around the azimuth. The rings are displaced vertically according to the mean flow through the disc but the centre of the rings is positioned so that the crossing point on the blade in plan view and the crossing angle of the ring to the blade corresponds to the intersection of a cycloidal wake.

The flow field from the helicopter fuselage has recently been recognised as an important source of additional loading around the front of the disc which can lead to blade stall in this region and an increase in vibration levels[3]. The fuselage flow field can be represented in the calculations and is normally calculated by a panel method originally developed for fixed wing aircraft.

The aerodynamic lift, drag and pitching moment coefficients are calculated by a method developed by Beddoes[4]. The effects of unsteady aerodynamics below stall are determined by Wagner functions, and a time delay model is used for the dynamic stall process.

The comparison between theory and flight has been made using the measured root flapping motion, shaft tilt, and advance ratio to define the input to the calculations. The rotor thrust was assumed to be the same as the weight of the aircraft as the forces on the fuselage were not known.

The comparisons of the flap and lag bending moments were made by subtracting the steady component from both the measured and calculated values because the datum is different in the two cases, thus the figures show only the oscillatory components. The torsion moments, however, for both measurement and calculation include the steady term.

The inclusion of unsteady aerodynamic effects has had a profound effect on the ability to predict rotor loads near the limits of the flight envelope. The accuracy of the method in predicting the torsional behaviour of the blades is illustrated in Fig 5 where the results of the calculations are compared with measurements from the Puma flight tests for an unstalled and stalled case at similar advance ratios. The calculated torsional moment for the unstalled case, Fig 5a, slightly overestimates the peak-to-peak amplitude of the oscillation, and there is some discrepancy in the third and fourth quadrants, but the agreement is good overall. The stalled example, Fig 5b, shows a more extreme case. The blade first stalls at about $\psi = 195^{\circ}$, but this is not due to the fuselage upwash around the front of the disc since theory predicts stall even when the fuselage is not represented. The blade continues to oscillate at its natural torsional frequency stalling again at $\psi = 260^{\circ}$ and $\psi = 330^{\circ}$. Theory predicts the phasing of the oscillation very well although the experimental results suggest that there is more damping present. The tip of the blade in this example twists 4.6° nose up at $\psi = 40^{\circ}$ to 3.2° nose down at $\psi = 290^{\circ}$. The ability to predict behaviour of this type allows pitch link load fatigue limits and hence flight envelope limits to be defined with confidence.

Two comparisons of the measured and calculated flatwise bending moments are shown in Fig 6. The trends at low speed, Fig 6a, are fairly well reproduced although there are differences in the magnitude and phasing of the high order bending modes. The differences however become more serious at high speed, Fig 6b, particularly around the disc from an azimuth angle of 120° through to 270°. The reason for this may be due to the vertical displacement of the tip vortex from the preceding blade. The front of the disc is generally a region of low downwash velocity, or even an upwash velocity at high speed, which will tend to keep the preceding blade tip vortex close to the plane of the rotor. This is not represented in the current vortex ring downwash model in which all the rings are displaced vertically according to the mean downwash velocity. Similarly, the tip vortices over the rear of the disc will be transported away from the disc more quickly than the mean downwash velocity and this will undoubtedly affect the blade loads from the retreating side around to the advancing side of the disc. A closer examination of the flight tests will prove useful in investigating the problem. The loads on the blades are known approximately from the leading edge pressure measurements thus the strength of the trailed vorticity can be determined. A simple analysis should then be able to give some indication of the

separation between the following blade and the tip vortex. Parallel work using the performance calculation could also be made to see the effect of changing the vertical separation of the rings by assuming that the vortex had passed through some representative velocity field, perhaps, for simplicity, that given by the Glauert formula.

A comparison of the calculated edgewise bending moments at low speed is shown in Fig 7a. The overall agreement is generally satisfactory considering that edgewise bending moments are notoriously difficult to calculate. There is some discrepancy in the third quadrant but changing the vertical separation of the vortex rings in this region may improve the correlation. The second example, Fig 7b, shows the edgewise bending moment for a stalled case. The agreement is less satisfactory and this may reflect the difficulty of calculating the aerofoil drag in separated flow conditions.

A new performance calculation is currently being developed which should provide a significant advance over the existing method. The major changes to be introduced are a new method of calculating the blade modes and a completely new model of the rotor dynamics. The new modal calculation now calculates modes with external forces representative of the mean conditions in flight, thus the modal displacements in the performance calculation now become small perturbations about the mean conditions. The new dynamic model, developed by Hansford at WHL, considers a generally curved blade and is correct to second order. These advances allow a much wider range of blade geometry to be studied than was possible before, and the inclusion of secondary load paths in the calculation means that new hub designs such as 'Starflex' type systems can now be evaluated. In addition, the modelling of dynamic stall has been improved[5].

4 REPRESENTATIVE AERODYNAMIC RESULTS

Before making any quantitative assessments of incidence and stall for comparison with prediction it is instructive to look at some samples of the data hard-copied from the VDU. One form of data presentation is the multiple sensor plot which gives the azimuthal variation of the leading edge (or trailing edge) pressure coefficient for one complete revolution. Such plots are shown in Fig 8a-d for a range of increasing advance ratio at a medium thrust coefficient. The position of the zero pressure coefficient in these plots corresponds directly with its radial location along the blade. The curves may be thought of notionally as plots of incidence, positive upwards. The features that are immediately obvious are the increasing amplitude of the basic sinusoidal variation with advance ratio and the superposition of well defined ripples and ridges which are due to rapid local changes in blade incidence as that part of the blade passes over a tip vortex. In regions where the ripples are sharply defined it is possible to locate the azimuthal position of the vortex to a high degree of accuracy. Two further points should be noted: the scale sensitivity is low to minimise overlap and the plots of inboard pressure may be unreliable at high advance ratio in the region of 270^{o} azimuth because of the low value of pressure to be measured.

Trailing edge pressure coefficients have not been included in the figure because of the absence of stall at the flight conditions given.

The leading and trailing edge pressure coefficients are included in Fig 9a&b for a flight condition at high thrust coefficient obtained at reduced rotor speed, high weight, and high altitude. The advance ratio (forward speed) was the maximum attainable within the extended flight envelope. By comparison with the leading edge pressures of the previous figure the large area of retreating blade stall evidenced by the collapse and ruggedness of the curves is immediately apparent. This is also reflected in the corresponding plots of

trailing edge pressure where fluctuating pressure divergence occurs over the same general area of the rotor disc. Corresponding plots of leading and trailing edge pressure at 79.5% radius (Fig 9c&d) but with an expanded vertical scale are also shown. The collapse of leading edge suction in the region of 200^{o} azimuth followed by gross trailing edge pressure divergence is immediately obvious.

It was observed from this sample and from the results in general that the local effects of blade-vortex interaction were more pronounced at high thrust coefficient.

5 BLADE-TIP VORTEX INTERACTION

The location of the vortex rings used in the wake model as described in section 3 give blade vortex crossing points in plan view that are identical with the tip path crossing points. However, it is by no means certain that this is actually what is required. The effective trail point of the tip vortex may be considerably inboard of the tip. The rotor is not a simple disc, but is coned, and induced velocities in the plane of the rotor (assumed zero in the present wake model) may be present due to wake distortion. With the measured variations of leading edge pressure, as given in Figs 8 and 9, giving a clear indication of vortex positions, it is now possible to check on the adequacy of the assumed wake geometry.

Fig 10a shows the locus of blade-vortex intersections in plan view at an advance ratio of 0.17 as given by the wake model assuming simple cycloidal vortex paths originating from the blade tip. It should be emphasised that actual intersection of the core with the blade is not implied as the vertical displacement is unspecified. The direction of each vortex core is indicated by the arrows and the direction of circulation follows a right-hand rule. Results for the higher advance ratio of 0.32 are given in Fig 10b. The loci from Fig 10 have been superimposed on the corresponding flight results in Fig 11. The strong overall correlation with ripple pattern is obvious but some discrepancy in phasing is also present.

Comparisons of the predicted blade-vortex intersections with flight results in polar form are given at two advance ratios and two widely different values of thrust coefficient in Figs 12 to 15a. In plotting the flight results, the point of inflexion of each 'ripple' has been taken to represent the blade-vortex crossing point. The key to the curves is given in Fig 10a with the thick curves representing flight results. At both advance ratios there is a difference between flight and prediction which increases towards the rear of the rotor disc suggesting that the vortex geometry is varying with time and has no permanent form in space. The discrepancy is more marked at the higher thrust coefficient. There are, however, other possible explanations for these differences, one of which is the presence of left sideslip. The discrepancy can be minimised by rotating the axis of the flight results as shown in Fig 15b to accord with a notional 12^{o} of left sideslip (note that the actual direction of rotation of the Puma rotor is contrary to the notation used in the figures). It should be emphasised that there is no direct evidence for a shift of this magnitude although, as mentioned in section 2, retrospective flight tests indicate 2^{o} of left sideslip to be present during similar tests without retreating blade stall at this advance ratio. The 10^{o} of additional sideslip required and notionally attributable to additional tail rotor thrust to trim appears excessively large. As mentioned previously further tests are required to clarify the position before differences are attributed completely to wake distortion.

A further possible cause for the discrepancy is that the tip vortex does not actually originate at the extreme tip, or that there is some wake

contraction. Fig 16 shows the locus of intersection of the blade with the vortex from the immediately preceding blade, which causes the major local changes in blade incidence, assuming the origin is inboard at 95% radius. At both advance ratios the effect is to move the loci towards the rear of the rotor disc by a significant amount. Also shown is the sensitivity to change in forward speed. The effect of a 5 knot increase is shown and as the speed of the helicopter during the flight tests is known to within 2 knots even when sideslip is present, errors from this source are considered minimal.

The evidence accumulated so far suggests that a closer correlation of blade-tip vortex locations in plan with flight results might be obtained by placing the origin of the assumed cycloidal vortex paths somewhat inboard of the tip. A more comprehensive analysis of a variety of test results over a range of advance ratios and thrust coefficients will be required to verify this and also indicate the necessity for any other changes in wake modelling.

The extent of blade stall can be deduced from the flight tests by examining the distribution of measured pressures. Points at which there is a collapse of leading edge suction, trailing edge pressure divergence, and reversion to attached flow have been superimposed on the polar plots, Figs 13 and 15a. For the two advance ratios under discussion this occurs only in the case of the higher thrust coefficient. It will be seen that at the lower advance ratio the stall first appears in the region of induced upwash from the vortex from the preceding blade shortly after 180^{o} azimuth and is largely confined to the third quadrant. At the higher advance ratio the initial collapse in leading edge suction is initially associated with the preceding blade vortex occurring towards the end of the second quadrant. Eventually the outer part of the blade well away from the tip vortex stalls early in the third quadrant, continuing in this condition until the end of the fourth quadrant. Unfortunately, in this flight the inner trailing edge pressure transducers were inoperative so there is less precision on the inward limit of detached flow.

6 COMPARISON OF PREDICTED AND MEASURED BLADE INCIDENCE

The blade loading has been calculated using the vortex ring wake model at two advance ratios and at the lower of the two values of thrust coefficient. The rotor was unstalled and estimated sideslip error small in these conditions so the agreement between theory and experiment should be close. The calculations provide values of predicted blade incidence and consideration is now given as to how these can be compared with the flight test results.

First of all it is useful to make a purely qualitative check on theory by comparing the azimuthal variation of predicted incidence directly with the variation of measured leading edge pressure coefficient. This is done in Fig 17 at 80% radius, for the two values of advance ratio. At the lower advance ratio, Fig 17a, theory predicts a disturbance due to the advancing blade passing over a tip vortex, but this comes at a larger value of azimuth than for the measured disturbance and is not as clearly defined. This confirms what was shown in Fig 12. There is a peak in the measured pressure coefficient, and in predicted incidence, at about 230^{o} azimuth, due again to the vortex from the previous blade, with a second smaller peak at about 270^{o} azimuth due to crossing the vortex from the opposite blade tip. The overall form of the predicted variation of incidence is very similar to the measured variation of leading edge pressure coefficient. The same comment applies at the higher advance ratio, Fig 17b, although there are fewer pronounced features here.

To make a more quantitative comparison of theory and experiment the leading edge pressures must be converted to incidence, or vice versa. As stated earlier, such a conversion should account for oscillatory effects and

use is therefore made of the recent oscillatory tests made at the Aircraft Research Association, UK, on a NACA 0012 aerofoil. Although this is not identical with the Puma blade section, which is effectively a NACA 0011.4 profile with a trailing edge tab added, the differences are not such as to produce significant errors in the conclusions reached. Thus, with the aid of the two-dimensional oscillatory aerofoil test results, an attempt will be made to evaluate the real blade incidence at 80% radius for azimuth angles of 90°, 270°, 0° and 180°, at $\mu = 0.32$. The values of incidence deduced can then be compared with those given by theory. At the same time, the predicted values of incidence can be used to deduce the corresponding value of leading edge pressure for comparison with the measured value.

At 90° azimuth, and 80% radius, theory predicts a value of incidence of -0.35°, and the predicted variation of lift coefficient with incidence (centred on 90° azimuth) is shown in Fig 18a. The blade Mach number at 90° azimuth is 0.7, and Fig 18a also shows the variation of C_L with α for a two-dimensional aerofoil test case at an appropriate combination of reduced frequency, amplitude and mean incidence, at $M = 0.7$. The aim here was to find the closest possible match of α, $\dot{\alpha}$ and $\ddot{\alpha}$ with those given by theory. Fig 18b gives the corresponding variation of leading edge pressure coefficient with incidence obtained from the oscillatory aerofoil test. Although the match between theoretical and oscillatory test conditions is very close, it is not precise and the value of incidence for the oscillatory test that corresponds to the value of C_L predicted at 90° is -0.2°. At this value of incidence, the value of C_p at 2% chord is -0.2 compared with a value of -0.5 measured on the rotor, indicating a significant error. Results from a further oscillatory aerofoil test case, selected again to give the closest match of α, $\dot{\alpha}$ and $\ddot{\alpha}$, are shown in Fig 18c&d. Here, the value of -0.5 for C_p at 90° azimuth, as measured in flight, corresponds to an incidence of about 1° and a value of C_L of about 0.25. The error between the predicted and actual incidence, and aerodynamic loading, thus seems to be quite large in this particular region of the disc.

The predicted peak incidence of 10° comes at 270° azimuth where the blade Mach number is very close to 0.3. Thus the two-dimensional aerofoil data, at $M = 0.3$, presented in Fig 2 help to evaluate the expected peak magnitude of C_p at 2% chord. The variation of C_p with α is shown for an oscillatory case and also for a quasi-static case (actually obtained in oscillatory conditions but with a frequency as low as 2 hertz where oscillatory effects are negligible). Although the incidence goes well above 10° in the oscillatory aerofoil case, it is seen that the quasi-static data gives an approximate guide to the maximum magnitude of C_p, producing only a small underestimate. Making some allowance for this, the peak value of C_p, corresponding to a maximum incidence of 10° can be estimated as -4.3 which can be compared with the measured value of -4.7. This suggests that theory underestimates the peak incidence by between 0.5° and 1°. However, this is a fairly small error for the retreating blade incidence, and may in any case be attributable to the fact that the two-dimensional data in Fig 2 were obtained on a slightly thicker aerofoil section than that on the rotor blade.

The results at azimuth angles of 0° and 180°, Fig 17b, show that the measured value of C_p is greater in magnitude at 0°, whereas the predicted incidence is greater at 180°. These two features, however, are quite compatible in oscillatory conditions, as seen in the two-dimensional results in Fig 3 at the appropriate Mach number of 0.5. With the aid of the data in Fig 3, the measured values of C_p can be taken to indicate incidences of about 5° and 6° at azimuth angles of 0° and 180° respectively, compared with the predicted values of 5.3° and 6.0°.

The foregone examples are instructive in showing the correlation of incidence through flight and section tunnel tests with those predicted, and are particularly useful when trends can be established over a range of results.

7 CONCLUDING REMARKS

The aim of the present paper has been to describe and discuss the current helicopter rotor aerodynamic and structural load measurements at RAE using the Puma as a test vehicle, to compare with prediction and where possible interpret and comment on deficiencies. Overall the results show an increasing confidence in the ability to predict detailed rotor aerodynamic performance and loads, even at conditions beyond normal rotor operating limits.

Modifications to UK prediction methods are continuing particularly with regard to a more comprehensive representation of blade dynamics and to improvements in the wake model guided by the flight results.

Extension to manoeuvring flight in recognition of the increased requirement for 'agility' and the possibility of a future air combat role are among future objectives.

REFERENCES

1) P. Brotherhood and M.J. Riley, Flight experiments on aerodynamic features affecting helicopter blade design, *Vertica*, Vol 2, pp 27-42 (1978) Pergamon Press.

2) J.C. Hubolt and G.W. Brooks, Differential equations of motion for combined flapwise bending chordwise bending and torsion of twisted nonuniform rotor blades, NACA Report 1346 (1958).

3) P.G. Wilby, C. Young and J. Grant, An investigation of the influence of fuselage flow field on rotor loads and the effects of vehicle configuration, Paper presented at the Fourth European Rotorcraft and Powered Lift Aircraft Forum, Stresa, Italy, September 1978.

4) T.S. Beddoes, A synthesis of unsteady aerodynamic effects including stall hysteresis, Paper presented at the First European Rotorcraft and Powered Lift Aircraft Forum, Southampton, England, September 1975.

5) T.S. Beddoes, Onset of leading edge separation effects under dynamic conditions and low Mach number, AHS Paper 78-63.

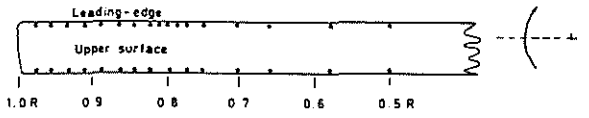

Fig 1 Distribution of pressure transducers on instrumented blade

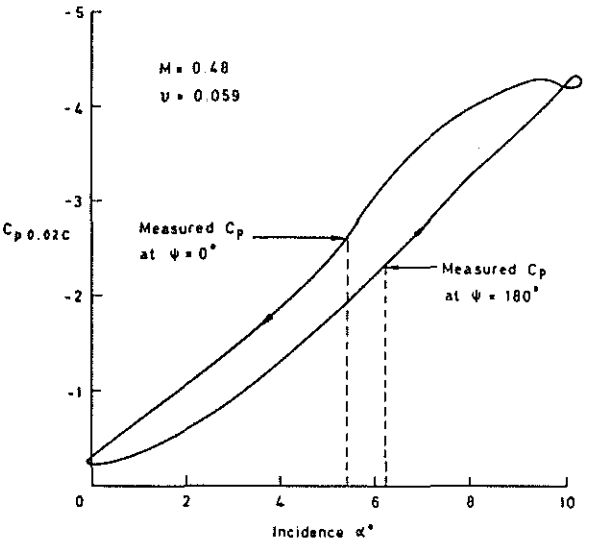

Fig 2 Variation of pressure coefficient at 2% and 90% chord for NACA 0012 section with attached flow, from oscillatory aerofoil tests at M = 0.29

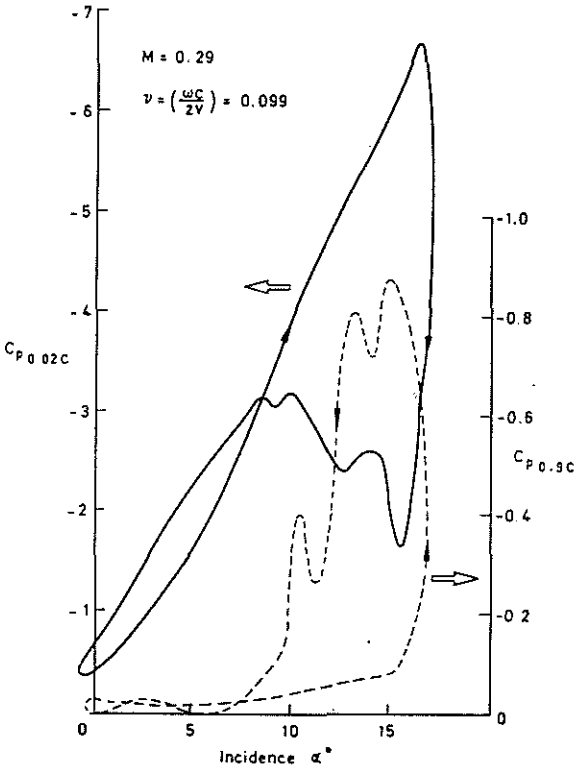

Fig 3 Variation of pressure coefficient at 2% chord on NACA 0012 aerofoil, from oscillatory tests at M = 0.48

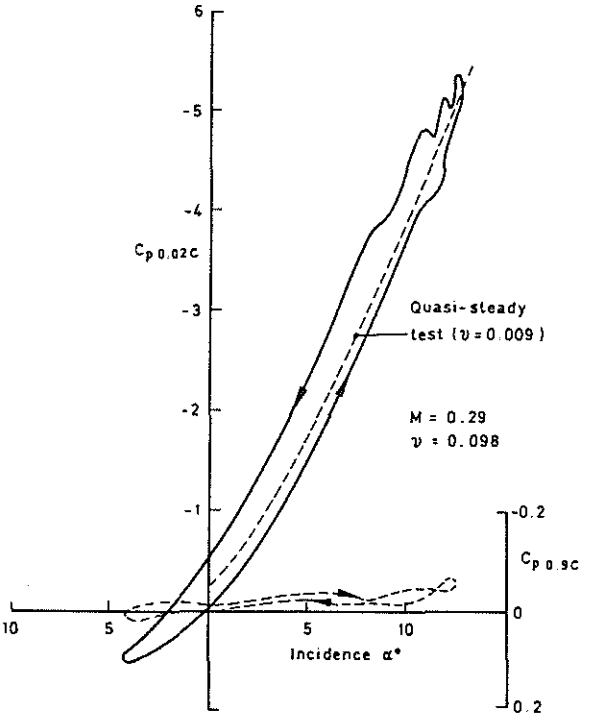

Fig 4 Variation of pressure coefficient at 2% and 90% chord for NACA 0012 section, during dynamic stall, from oscillatory aerofoil tests

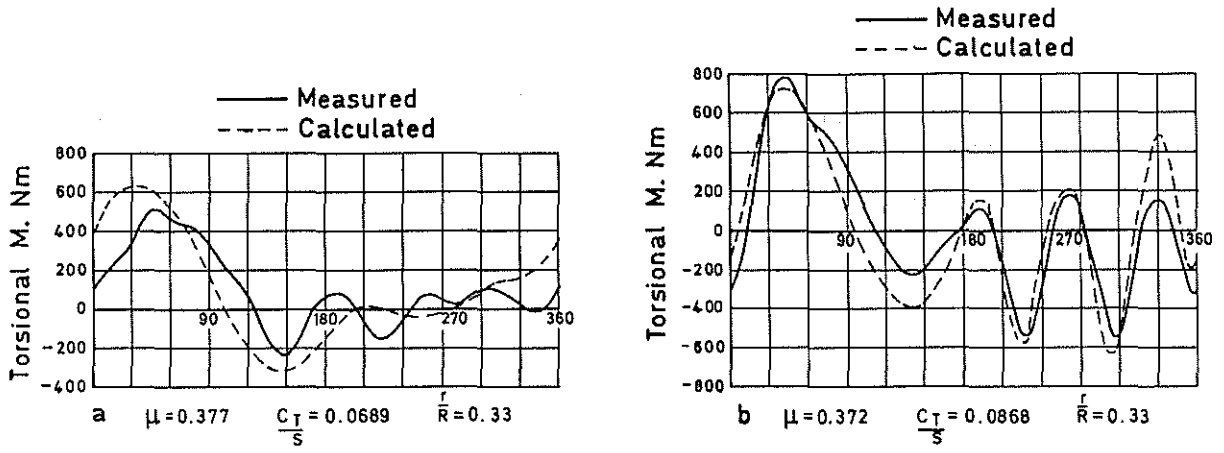

Fig 5 Measured and predicted torsional moment

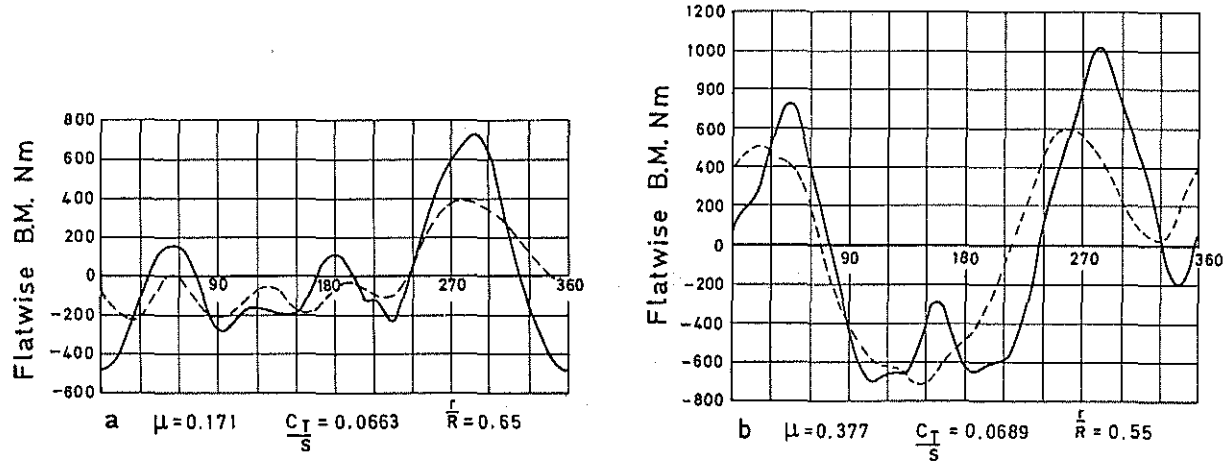

Fig 6 Measured and predicted flatwise bending moment

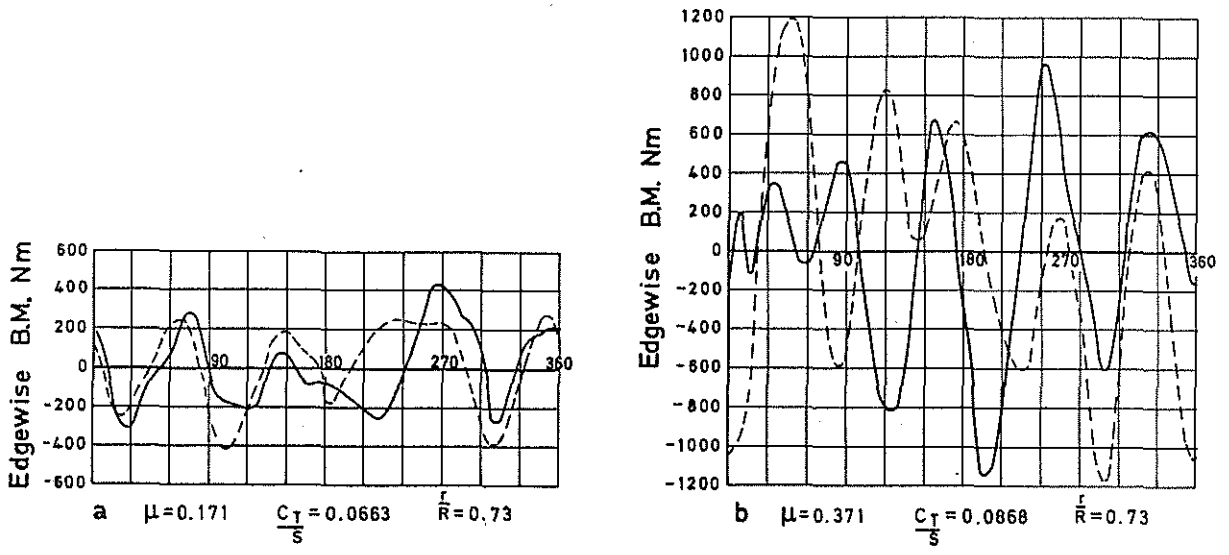

Fig 7 Measured and predicted edgewise bending moment

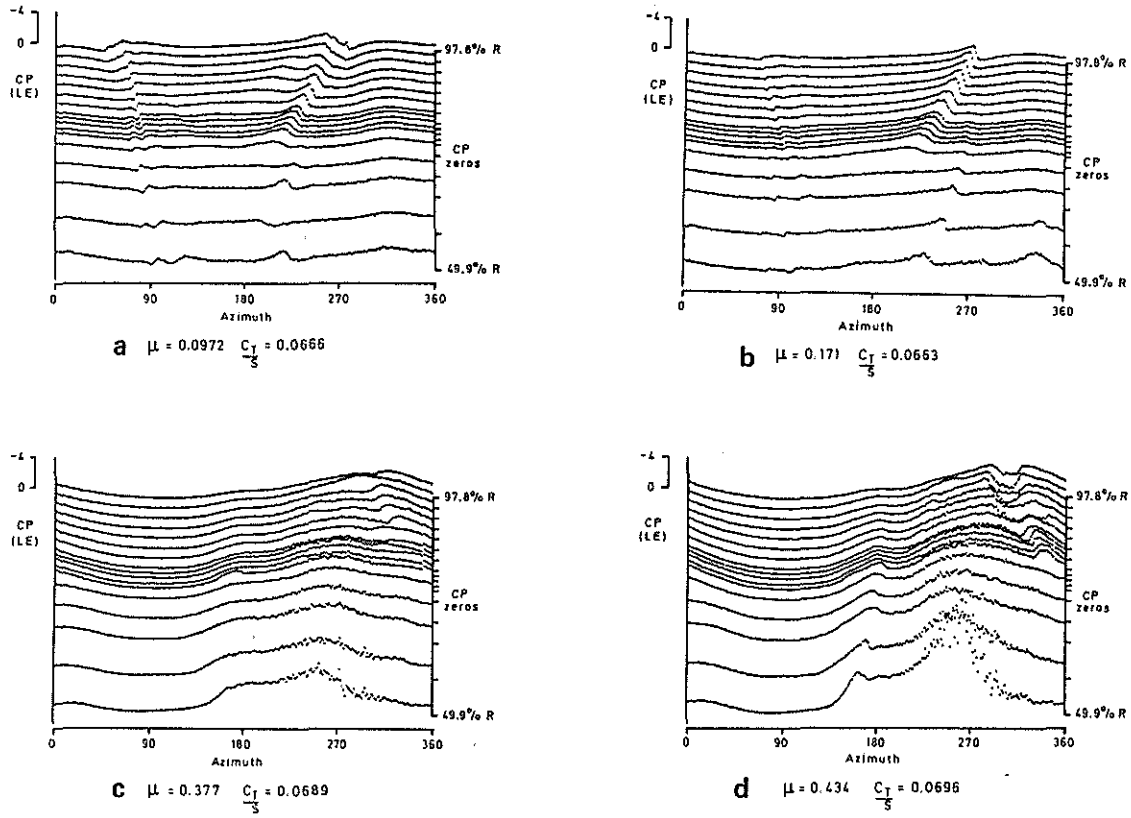

Fig 8 Variation of LE pressure coefficient with advance ratio at medium thrust coefficient

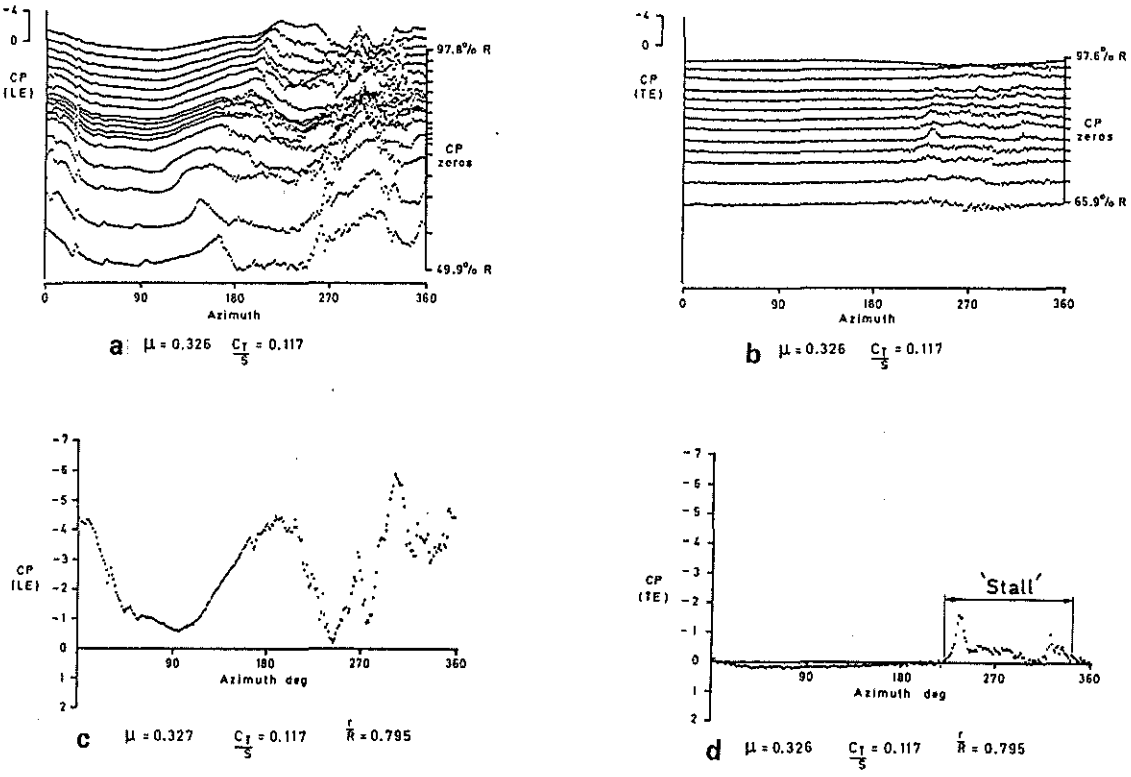

Fig 9 LE and TE pressure coefficients at high thrust coefficient and pronounced stall

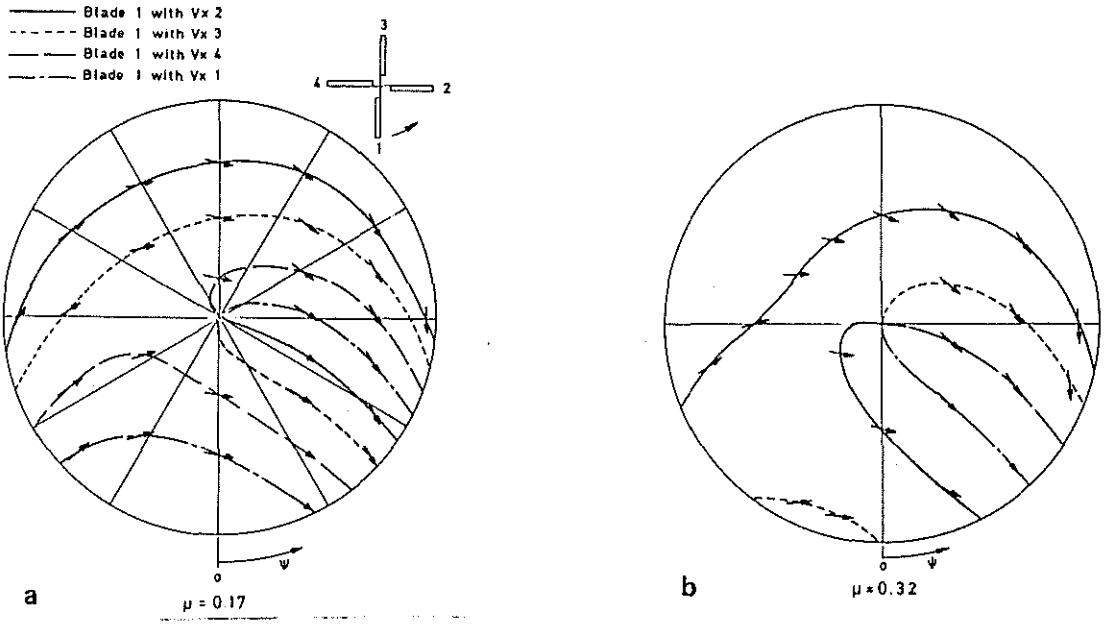

Fig 10 Predicted loci of blade-vortex intersections (plan-view)

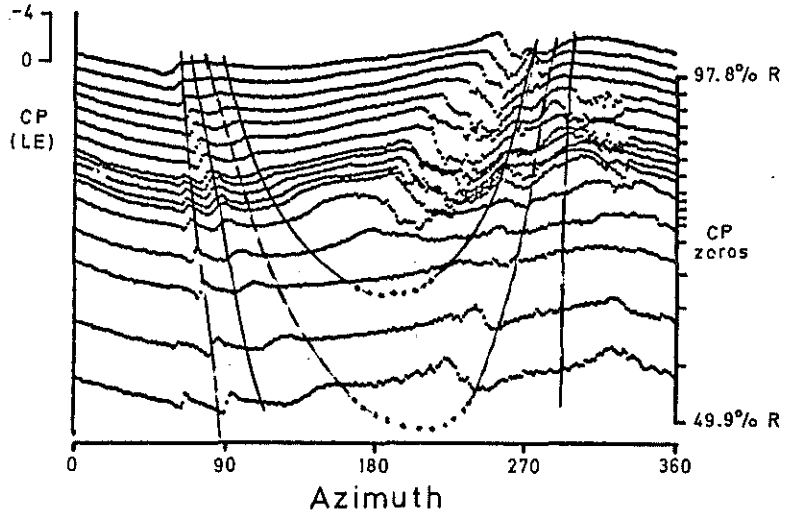

Fig 11 Superposition of blade-vortex intersection loci on LE pressure coefficients, $\mu = 0.175$, $\frac{C_T}{S} = 0.11$

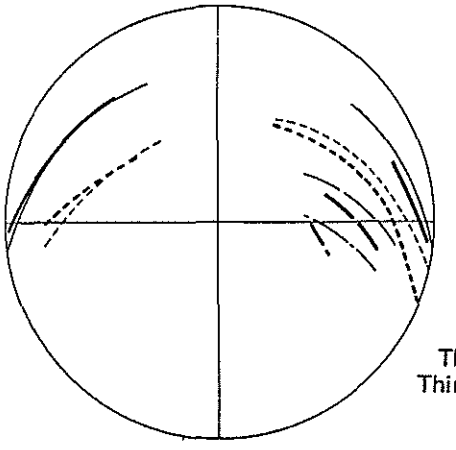

Thick curves flight
Thin curves prediction
Key as Fig 9a

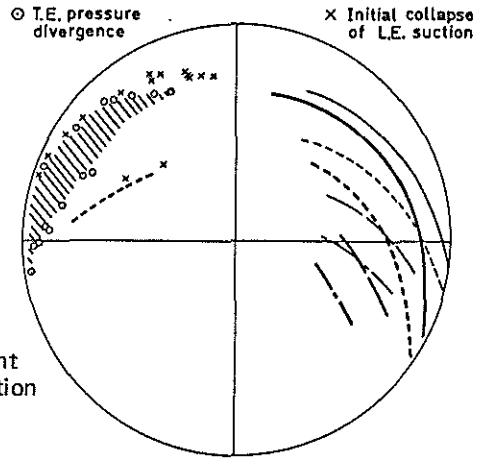

Fig 12 Comparison of measured and predicted loci, $\mu = 0.17$, $\frac{C_T}{S} = 0.066$

Fig 13 Comparison of measured and predicted loci, $\mu = 0.17$, $\frac{C_T}{S} = 0.12$

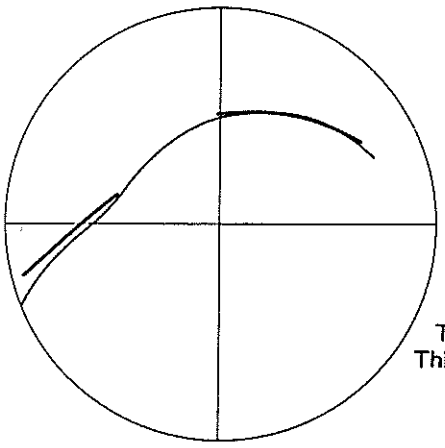

Fig 14 Comparison of measured and predicted loci, $\mu = 0.32$, $\frac{C_T}{S} = 0.066$

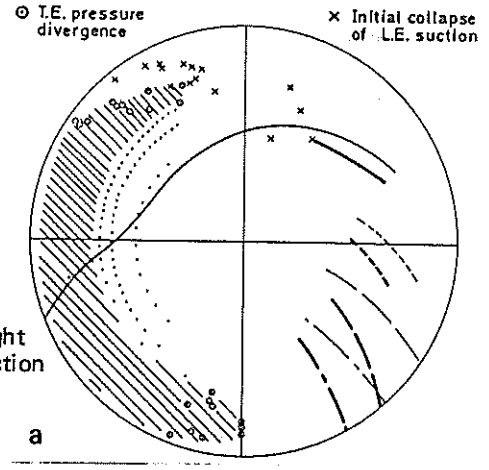

a

Fig 15a Comparison of measured and predicted loci, $\mu = 0.32$, $\frac{C_T}{S} = 0.32$

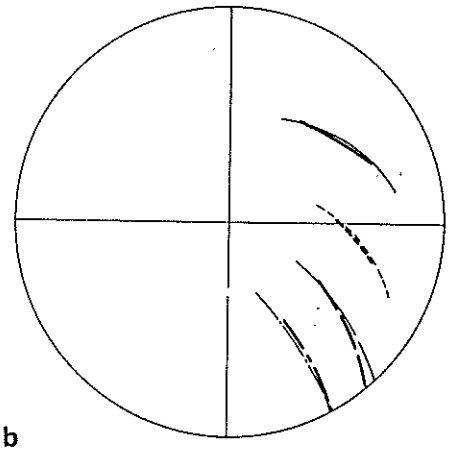

b

Fig 15b Conditions as at 15b but with 12° port sideslip assumed

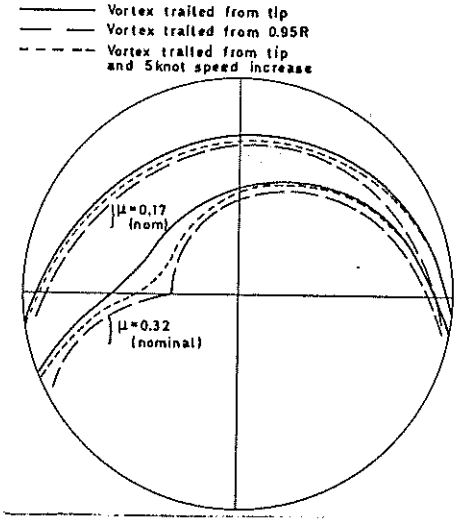

Fig 16 Predicted loci of intersection of blade with vortex from preceding blade showing effects of change in trail origin and speed increment

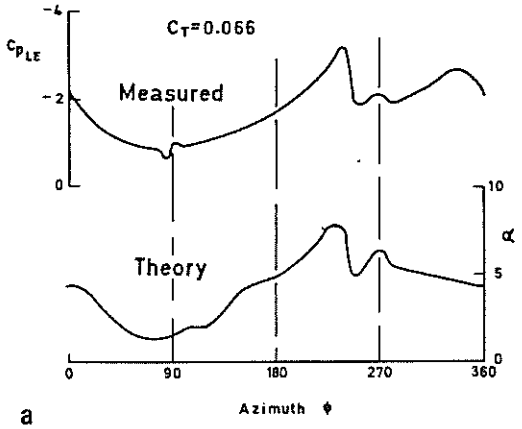

a

Fig 17a Measured azimuthal variation of pressure coefficient at 2% chord, and predicted variation of incidence, for 80% radius and $\mu = 0.17$

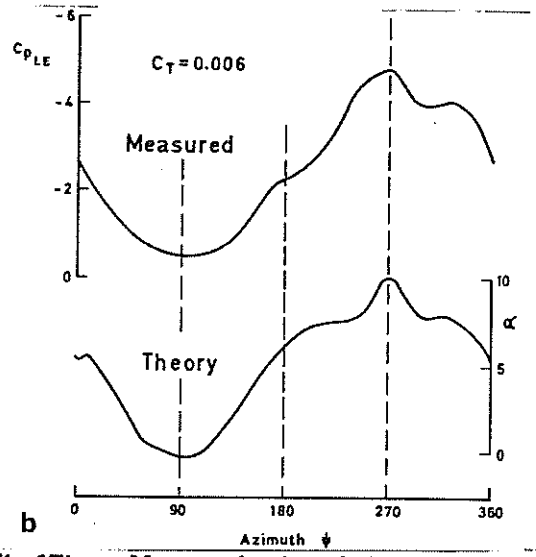

b

Fig 17b Measured azimuthal variation of pressure coefficient at 2% chord, and predicted variation of incidence, for 80% radius and $\mu = 0.32$

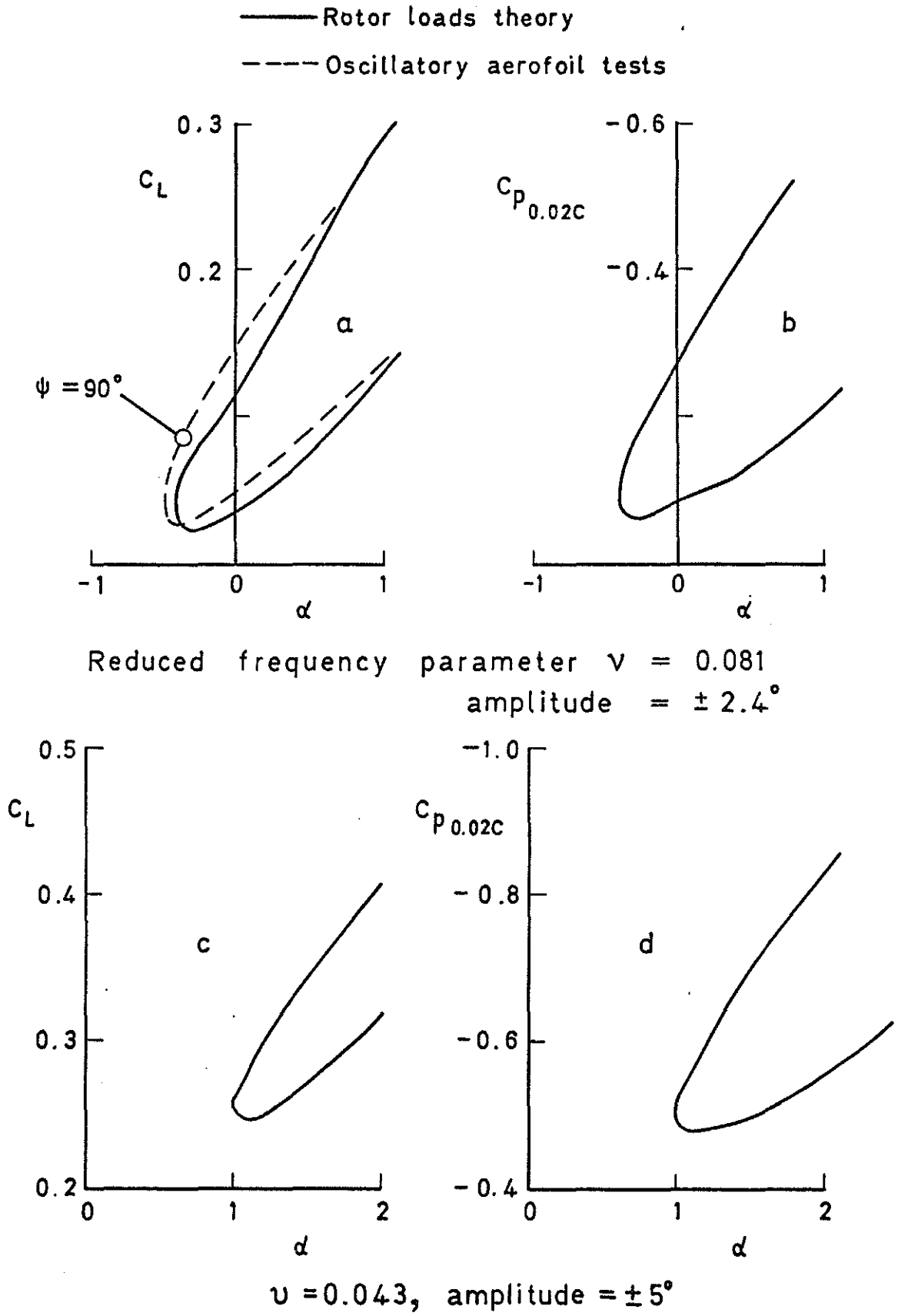

Fig 18 Predicted variation of C_L with incidence through 90° azimuth, and oscillatory aerofoil test data at M = 0.69